

Poisson Variational Autoencoder

Hadi Vafaii¹
vafaii@berkeley.edu

Dekel Galor¹
galor@berkeley.edu

Jacob L. Yates¹
yates@berkeley.edu

¹UC Berkeley

Abstract

Variational autoencoders (VAE) employ Bayesian inference to interpret sensory inputs, mirroring processes that occur in primate vision across both ventral [1] and dorsal [2] pathways. Despite their success, traditional VAEs rely on continuous latent variables, which deviates sharply from the discrete nature of biological neurons. Here, we developed the Poisson VAE (\mathcal{P} -VAE), a novel architecture that combines principles of predictive coding with a VAE that encodes inputs into discrete spike counts. Combining Poisson-distributed latent variables with predictive coding introduces a metabolic cost term in the model loss function, suggesting a relationship with sparse coding which we verify empirically. Additionally, we analyze the geometry of learned representations, contrasting the \mathcal{P} -VAE to alternative VAE models. We find that the \mathcal{P} -VAE encodes its inputs in relatively higher dimensions, facilitating linear separability of categories in a downstream classification task with a much better ($5\times$) sample efficiency. Our work provides an interpretable computational framework to study brain-like sensory processing and paves the way for a deeper understanding of perception as an inferential process.

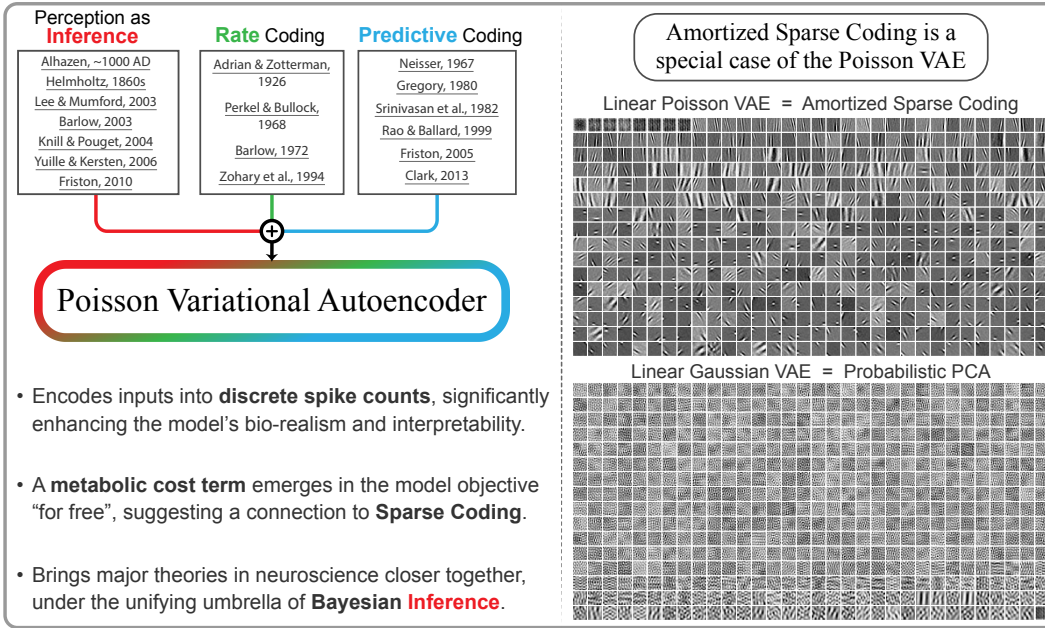


Figure 0: Graphical abstract. Introducing the Poisson Variational Autoencoder (\mathcal{P} -VAE), which draws on key concepts in neuroscience. When trained on natural image patches, \mathcal{P} -VAE with a linear decoder develops Gabor-like feature selectivity, reminiscent of Sparse Coding [3]. In sharp contrast, the standard Gaussian VAE learns the principal components [4].

1 Introduction

The study of artificial neural networks (ANN) and neuroscience has always been closely linked, driving advancements in both fields [5–10]. Despite the close proximity of the two fields, most ANN models deviate substantially from biological brains [11, 12]. A major challenge is designing models that not only perform well computationally but also exhibit “brain-like” structure and function. This is seen both as a goal for improving ANNs [13–15], and better understanding biological brains [8, 9, 16–19], which has recently been referred to as the *neuroconnectionist* research programme [20].

Drawing from neuroscience, a major guiding idea is that perception is a process of inference [21, 22], where the brain constructs a representation of the external world by inferring the causes of sensory inputs [23–26]. This concept is mirrored in “generative AI” where models learn the generative process underlying their inputs [27–29]. However, in this vein, there is a tension between small well-understood models that are directly inspired by cortex, such as sparse coding [3] and predictive coding [30], and deep generative models that perform well [31–34].

The variational autoencoder (VAE; [35, 36]) model family is a promising candidate for neuroconnectionist goals for multiple reasons. First, VAEs learn probabilistic generative models of their inputs and are grounded in Bayesian probability theory, providing a solid theoretical foundation that directly incorporates the concept of perceptual inference [10, 22]. Second, the VAE model family, specifically hierarchical VAEs, is broad with other generative models, such as diffusion models, understood as special cases of hierarchical VAEs [37–39]. Finally, VAEs learn representations that are similar to cortex [1, 2, 40], exhibit cortex-like topographic organization [41, 42], and make perceptual errors that mimic those of humans [43], indicating a significant degree of neural, organizational, and psychophysical alignment with the brain.

However, standard VAEs diverge from brains in the way they encode information. Biological neurons fire all-or-none action potentials [44], and are thought to represent information via firing rate [45–49]. These firing rates must be positive and generate discrete “spike” counts, which exhibit conditionally Poisson-like statistics in small counting windows [49–51]. In contrast, VAEs are typically parameterized with real-valued, continuous, Gaussian distributions [52].

Contributions. In this work, we address this discrepancy by introducing the Poisson Variational Autoencoder (\mathcal{P} -VAE), a novel architecture that combines perceptual inference with two other inspirations from neuroscience (Fig. 0). First, that information is encoded in the rates of discrete spike counts, which are approximately Poisson-distributed on short time intervals. And second, that feedforward connections encode deviations from expectations contained in feedback connections (Fig. 1a; [30, 53]). We introduce a reparameterization trick for Poisson samples (Algorithm 1), and derive the evidence lower bound (ELBO) objective for the \mathcal{P} -VAE (eq. (3)). Overall, we believe \mathcal{P} -VAE introduces a promising new model at the intersection of computational neuroscience and machine learning that offers several appealing features over existing VAE architectures:

- The \mathcal{P} -VAE loss derivation (eq. (3)) naturally results in a metabolic cost term that penalizes high firing rates, such that \mathcal{P} -VAE with a linear decoder implements amortized sparse coding (Fig. 1b). We validate this prediction empirically.
- \mathcal{P} -VAE largely avoids the prevalent posterior collapse issue, maintaining many more active latents compared to alternative VAE models (Table 1), especially the continuous ones.
- \mathcal{P} -VAE encodes its inputs in relatively higher dimensions, facilitating linear separability of categories in a downstream classification task with a much better ($5\times$) sample efficiency.

We evaluate these results on two natural image datasets and MNIST. The \mathcal{P} -VAE paves the way for the future development of interpretable hierarchical models that perform “brain-like” inference.

2 Background & Related work

Perception as inference: connections to neuroscience and machine learning. A centuries-old idea [21, 22], “perception as inference” argues that coherent perception of the world results from the unconscious inference over the causes of the senses. In other words, the brain learns a generative model of the sensory inputs. This has led to fruitful theoretical work in neuroscience [23, 54, 55] and machine learning [56, 57], including VAEs [52]. See Marino [10] for a review.

Efficient, predictive, and sparse coding. Another longstanding idea in neuroscience is that brains are adapted to the statistics of the environment. Efficient coding states that brains represent as much information about the environment as possible while minimizing neural resource use [58, 59].

Predictive coding [30, 60, 61] postulates that the brain generates a statistical prediction of its inputs, with feedforward networks carrying only the prediction errors or unexplained information [62]. More recently, ANNs based on predictive coding have been shown to capture a wide range of phenomena in biological neurons across the visual system [63, 64]. More broadly, prediction in time has emerged as an objective that lends itself to brain-like representations [65, 66].

Sparse coding (SC) is directly inspired by efficient coding, aiming to explain inputs as sparsely as possible [47, 67]. SC was the first unsupervised model to learn representations closely resembling the receptive fields of V1 neurons [3] and predicts an array of empirical features of neural activity [68–78]. SC is formalized with a generative model where neural activations \mathbf{z} are sampled from a sparsity-inducing prior, $\mathbf{z} \sim p(\mathbf{z})$, and the input image \mathbf{x} is reconstructed as a linear combination of basis vectors Φ , plus additive Gaussian noise, $\hat{\mathbf{x}} = \Phi\mathbf{z} + \varepsilon$. The SC loss is as follows:

$$\mathcal{L}_{\text{SparseCoding}}(\mathbf{x}; \Phi, \mathbf{z}) = \|\mathbf{x} - \Phi\mathbf{z}\|_2^2 + \beta\|\mathbf{z}\|_1. \quad (1)$$

Commonly used algorithms for sparse coding include the locally competitive algorithm (LCA; [79]), which is a biologically plausible algorithm to optimize eq. (1), and iterative shrinkage-thresholding algorithm (ISTA; [80, 81]), which has shown robust performance in learning sparse codes given a fixed dictionary Φ .

VAE objective. VAEs define a probabilistic generative model $p(\mathbf{x}, \mathbf{z})$, where \mathbf{x} denotes the observed data and \mathbf{z} are some latent variables. The generative process samples \mathbf{z} from a prior distribution $p(\mathbf{z})$ and then generates the observed data \mathbf{x} from the conditional distribution $p_{\theta}(\mathbf{x}|\mathbf{z})$, also known as the “decoder”. The “encoder”, $q_{\phi}(\mathbf{z}|\mathbf{x})$, performs approximate inference on the inputs. Model parameters are learned by maximizing the evidence lower bound (ELBO) objective, which is derived from variational inference (see appendix C for the full set of derivations). The ELBO is given by:

$$\log p(\mathbf{x}) \geq \mathbb{E}_{q_{\phi}(\mathbf{z}|\mathbf{x})} \left[\log p_{\theta}(\mathbf{x}|\mathbf{z}) \right] - \mathcal{D}_{\text{KL}}(q_{\phi}(\mathbf{z}|\mathbf{x}) \parallel p(\mathbf{z})) = \mathcal{L}_{\text{VAE}}(\mathbf{x}; \theta, \phi). \quad (2)$$

The first term captures the reconstruction performance of the decoder, and the second term, the “KL term”, captures the distance of the approximate posterior from the prior.

The specific form of these distributions is up to the practitioner. In standard VAEs, factorized Gaussians are typically used: $q = \mathcal{N}(\mathbf{z}; \mu(\mathbf{x}), \sigma(\mathbf{x})^2)$ and $p = \mathcal{N}(\mathbf{z}; \mathbf{0}, \mathbf{I})$. The likelihood, $p_{\theta}(\mathbf{x}|\mathbf{z})$, is also typically modeled as a Gaussian conditioned on a parameterized neural network $f_{\theta}(\mathbf{z})$.

Amortized inference in VAEs. A major contribution of VAEs is the idea of amortizing inference over the latents \mathbf{z} with a black box ANN [82, 83]. “Amortized” inference borrows a term from finance to capture the idea of spreading out costs—here, the cost of performing inference over multiple samples. In amortized inference, a neural network learns (during training) how to map a data sample to a distribution over latent variables given the sample. The cost is paid during training, but the trained model can then be used to perform inference on future samples efficiently. It has been argued that the brain performs amortized inference for computational efficiency [84].

VAEs connection to biology. VAEs have been shown to contain individual latents that resemble neurons, capturing a wide range of the phenomena observed in visual cortical areas [40] and human perceptual judgments [43]. Like many other ANN models [85, 86], VAEs have been found to learn representations that are predictive of single-neuron activity in both the ventral [1] and dorsal [2] streams. However, unlike most ANNs, the mapping from certain VAEs to neural activity is incredibly sparse, even one-to-one in some cases [1, 2].

Discrete VAEs. VAEs with discrete latent spaces, such as VQ-VAE [87] and Categorical VAE [88], are designed to capture complex data structures by mapping inputs to a finite set of latent variables. Unlike traditional VAEs that use continuous latent spaces, these models leverage discrete representations to enhance interpretability and can yield high performance with lower capacity [89].

Algorithm 1 Reparameterized sampling (rsample) for Poisson distribution.

Input:

$\lambda \in \mathbb{R}_{>0}^{B \times K}$ # rate parameter; B , batch size; K , latent dimensionality.
 n_{exp} # number of exponential samples to generate.
temperature # controls the sharpness of the thresholding.

```

1: procedure RSAMPLE( $\lambda, n, \text{temperature}$ )
2:    $\text{Exp} \leftarrow \text{Exponential}(\lambda)$                                  $\triangleright$  create exponential distribution
3:    $\Delta t \leftarrow \text{Exp.rsample}((n_{\text{exp}},))$                        $\triangleright$  sample inter-event times,  $\Delta t : [n_{\text{exp}} \times B \times K]$ 
4:   times  $\leftarrow \text{cumsum}(\Delta t, \text{dim}=0)$                            $\triangleright$  compute arrival times, same shape as  $\Delta t$ 
5:   indicator  $\leftarrow \text{sigmoid} \left( \frac{1 - \text{times}}{\text{temperature}} \right)$        $\triangleright$  soft indicator for events within unit time
6:    $z \leftarrow \text{sum}(\text{indicator}, \text{dim}=0)$                            $\triangleright$  event counts, or number of spikes,  $z : [B \times K]$ 
7:   return  $z$ 
8: end procedure

```

VAEs connection to sparse coding. Previous work has attempted to connect sparse coding and VAEs directly [90–92], with each approaching the problem differently. Geadah et al. [90] introduced sparsity-inducing priors (such as Laplace or Cauchy) and a linear decoder with an overcomplete latent space. Tonolini et al. [91] introduced a spike and slab prior into a modified ELBO, and Xiao et al. [92] added a sparse coding layer learned by ISTA to the latent space of a VQ-VAE. Notably, none of the three ended up minimizing the sparse coding loss. Two of the three maintain the linear generative model with an overcomplete latent space, but the ELBO in both requires an additional approximation step for the KL term [90, 91].

3 Theoretical results

Our main contribution is integrating Poisson-distributed latents into VAEs, where both the approximate posterior and the prior are parameterized as Poisson distributions. Critically, the latents z are no longer continuous variables, but rather they are discrete spike counts. To perform inference over discrete latents, we introduce a Poisson reparameterization trick. We then derive the KL term and obtain the full \mathcal{P} -VAE objective.

Poisson reparameterization trick. For a homogeneous Poisson process [93–95], given a window size $\Delta t = 1$, and rate λ , we can generate Poisson distributed counts by drawing randomly distributed wait-times from an exponential distribution with mean $1/\lambda$ and counting all events where the cumulative time is less than 1. Because the exponential distribution is trivially reparameterized [35], and PyTorch contains an implementation [96], we need only to approximate the hard threshold for comparing cumulative wait times with the window size. We accomplish this by replacing the indicator function with a sigmoid as in refs. [88, 97].

Algorithm 1 demonstrates the steps: Given a matrix of rates λ , sample n_{exp} wait times $t_1, t_2, \dots, t_{n_{\text{exp}}}$ for each element of λ by sampling from an exponential distribution with mean $1/\lambda(i)$. We then calculate the cumulative event times $S(n_{\text{exp}}) = \sum_{j=1}^{n_{\text{exp}}} t_j$, pass them through a sigmoid $\sigma(\frac{1-S}{\text{temperature}})$, and sum over samples to get event counts, z . The temperature controls the sharpness of the thresholding. We adaptively scale the number of samples, n_{exp} , by keeping track of the maximum rate in each batch, λ_{max} , and then use the inverse cumulative density function (cdf) for Poisson to find the number of samples, n_{exp} , such that $\text{cdf}(n_{\text{exp}}; \lambda_{\text{max}}) = 0.99999$.

\mathcal{P} -VAE architecture. The architecture of \mathcal{P} -VAE captures the interactions between feedforward and feedback connections that are present in all visual cortical areas [98]. Feedforward areas carry sensory information and feedback connections are thought to carry modulatory signals such as attention [53] or prediction [30], which interact multiplicatively with feedforward inputs [53, 99].

\mathcal{P} -VAE embodies this idea by having the posterior rates depend on the prior, such that $r_{\text{prior}} = \textcolor{blue}{r}$ and $r_{\text{post.}} = \textcolor{blue}{r} \delta \textcolor{red}{r}(x)$. See appendix C for the full derivations. The prior rates, $\textcolor{blue}{r}$, are learnable parameters that capture expectations about the statistics of the input. The encoder outputs $\delta \textcolor{red}{r}(x)$, which captures *deviations* from the prior. Thus, \mathcal{P} -VAE models the interaction between prior

expectations, and deviations from them, in a multiplicative and symmetric way. This results in a posterior, $q(z|x) = \text{Pois}(z; \mathbf{r}\delta\mathbf{r}(x))$, and prior, $p(z) = \text{Pois}(z; \mathbf{r})$, where z is the spike count variable. The general model architecture is shown in Fig. 1a.

\mathcal{P} -VAE loss function. For a comprehensive derivation of the \mathcal{P} -VAE objective, see appendix C. Here, we report the final result:

$$\mathcal{L}_{\text{PVAE}} = \mathbb{E}_{z \sim \text{Pois}(z; \mathbf{r}\delta\mathbf{r})} \left[\|\mathbf{x} - \text{dec}(z)\|_2^2 \right] + \sum_{i=1}^K \mathbf{r}_i f(\delta\mathbf{r}_i), \quad (3)$$

where $\text{dec}(\cdot)$ is the decoder neural network, and $f(y) := 1 - y + y \log y$ (see supplementary Fig. 7).

\mathcal{P} -VAE relationship to sparse coding. The KL term in eq. (3) penalizes firing rates. Both \mathbf{r} and $\delta\mathbf{r}$ are positive by definition, and $f(y) \geq 0$, strongly resembling the sparsity penalty in Olshausen and Field [3]. To make this connection more explicit, we make two additional assumptions (Fig. 1b):

1. The decoder is a linear generative model: $\hat{\mathbf{x}} = \Phi z$, with $\mathbf{x} \in \mathbb{R}^M$ and $\Phi \in \mathbb{R}^{M \times K}$.
2. The latent space is overcomplete: $K > M$.

Because both $\mathbb{E}_{z \sim \text{Pois}(z; \lambda)}[z_i]$ and $\mathbb{E}_{z \sim \text{Pois}(z; \lambda)}[z_i z_j]$ have closed-form solutions (eq. (17)), the reconstruction term in eq. (3) can be computed analytically for a linear decoder, resulting in:

$$\mathcal{L}_{\text{SC-PVAE}}(\mathbf{x}; \delta\mathbf{r}, \mathbf{r}, \Phi) = \|\mathbf{x} - \Phi \lambda\|_2^2 + \lambda^T \text{diag}(\Phi^T \Phi) + \beta \sum_{i=1}^K \mathbf{r}_i f(\delta\mathbf{r}_i). \quad (4)$$

where $\lambda = \mathbf{r}\delta\mathbf{r}(\mathbf{x})$ are the posterior firing rates, $f(y)$ is defined as above, and β is a hyperparameter that scales the contribution of the KL term, and changes the sparsity penalty for the \mathcal{P} -VAE.

The relationship between the linear \mathcal{P} -VAE loss (eq. (4)) and the sparse coding loss (eq. (1)) can now be seen. Both contain a term that minimizes the squared error of the reconstruction, and a term (two terms for \mathcal{P} -VAE) that penalizes non-zero firing rates. Unlike prior work that directly implemented amortized sparse coding [90, 91], here the activity penalty naturally emerges from the derivations, and the only additional assumption was an overcomplete linear generative model. The inference is accomplished using a parameterized feed-forward neural network, $\delta\mathbf{r}(\mathbf{x})$, thus, it is amortized. We call this specific case of \mathcal{P} -VAE “Amortized Sparse Coding” (Fig. 1b).

Note that a closed-form derivation of the reconstruction term is possible for any VAE with a linear decoder and a generating distribution that has a mean and variance (see eq. (18)).

This closed-form expression of the loss given a linear decoder is useful because we can see how different parameters contribute to the loss. Furthermore, we can compute gradients of the whole loss exactly, and use this to evaluate our Poisson reparameterization.

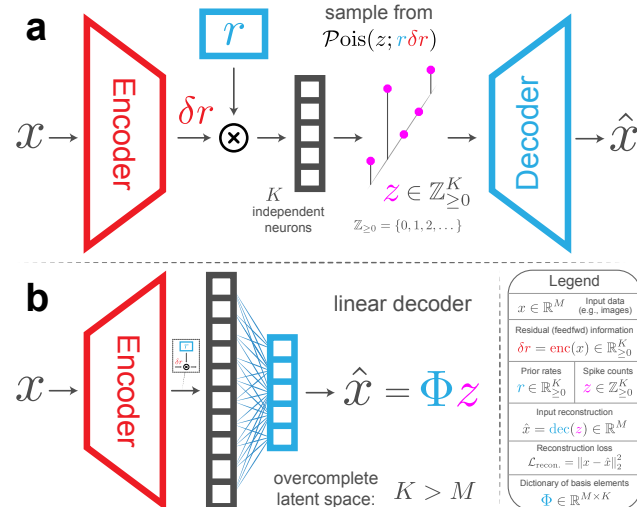


Figure 1: (a) Model architecture. Colored shapes depict learnable model parameters, including the prior firing rates, \mathbf{r} . We color code the model’s **inference** and **generative** components using **red** and **blue**, respectively. The \mathcal{P} -VAE encodes its inputs in discrete spike counts, z , significantly enhancing its biological realism. (b) “Amortized Sparse Coding” is contained as a special case of the \mathcal{P} -VAE.

Table 1: Models considered in this paper.

Discrete		Continuous	
Poisson VAE (\mathcal{P} -VAE)	Categorical VAE (\mathcal{C} -VAE; [88, 97])	Gaussian VAE (\mathcal{G} -VAE; [35, 36])	Laplace VAE (\mathcal{L} -VAE; [40, 90])

4 Experiments

To evaluate the \mathcal{P} -VAE, we perform three sets of experiments. First, we utilize the theoretical results for a linear decoder (eqs. (4) and (18)) to test the effectiveness of our reparameterization algorithm. We compare to alternative VAE models with established reparameterization tricks (e.g., Gaussian).

Second, to confirm \mathcal{P} -VAE with a linear decoder not only resembles amortized sparse coding, but practically performs like sparse coding, we compare to standard and well-established sparse coding algorithms such as the locally competitive algorithm (LCA; [79]) and the widely-used iterative shrinkage-thresholding algorithm (ISTA; [80, 81]) to see if \mathcal{P} -VAE reproduces their results.

Third, we test the \mathcal{P} -VAE in a generic representation learning context and evaluate the geometry of learned representations for downstream tasks. For these experiments, both the encoder and decoder’s architecture is a ResNet (see appendix A for full architecture and training details).

Alternative models. We compare \mathcal{P} -VAE to both discrete and continuous VAEs (Table 1). Other than the traditional Gaussian, we compare to Laplace-distributed VAEs because previous work found the Laplace distribution supported robust sparse representations [40, 90]. Additionally, we compare to Categorical VAEs, trained using the Gumbel-Softmax trick [88, 97]. We use PyTorch’s implementation which is based on Maddison et al. [97].

Finally, we test models where latents are Gaussian passed through an activation function before passing to the decoder. We call these models \mathcal{G} -VAE_{act}, where $\text{act} \in \{\text{relu}, \text{exp}\}$, but they capture other families of distributions (truncated Gaussian and log-normal). We include these to test the hypothesis that positive constraints (and not discrete latents) are the key contribution of Poisson [100].

Datasets. For sparse coding results, we use 101 natural images from the van Hateren dataset [101]. We tile the images to extract 16×16 patches and apply whitening and contrast normalization, as is typically done in sparse coding literature [3, 102]. To test the generalizability of our sparse coding results, we repeat these steps on CIFAR10 [103], a dataset we call CIFAR_{16×16}. For the general representation learning results, we use MNIST. See appendix A for additional details.

Statistical tests. In the VAE literature, it is known that random seeds can have a large effect compared to architecture or regularization [104]. Therefore, we train each configuration using 5 different random initializations. We report 99% confidence intervals everywhere, and perform paired *t*-tests, reporting significance for $p < 0.01$ (FDR corrected).

Training details. Because we considered a variety of architectures, training time is variable. We trained 195 VAE models, $n = 5$ seeds each, resulting in a total of $195 \times 5 = 975$ VAEs. For sparse coding models, we ran ISTA [80, 81] and LCA [79] with 270 hyperparameter combinations each. See appendix A for more details. Training all models took roughly a week on 8 RTX 6000 Ada GPUs.

Evaluating Poisson reparameterization. \mathcal{P} -VAE with a linear decoder has a closed form solution eq. (4), which lets us evaluate how well our reparameterized gradients perform compared to the exact ones. We compare our results to the gold-standard Gaussian as well as Categorical and Laplace VAEs. Table 4 shows the results. Monte-Carlo sampling with Poisson reparameterization closely matches exact inference just like established methods for Gaussian and Laplace. In contrast, the straight-through (ST; [105]) estimator performs poorly (see also supplementary Fig. 4).

The \mathcal{P} -VAE learns basis vectors similar to those from sparse coding. A major result from sparse coding is that it learns basis vectors (dictionaries) that resemble the “Gabor-like” receptive fields of

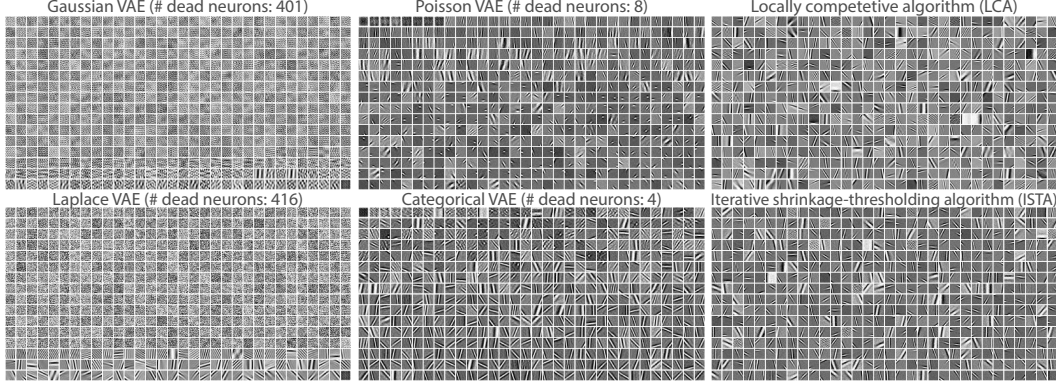


Figure 2: Learned basis elements, $K = 512$ total, each made of $16 \times 16 = 256$ pixels (i.e., $\Phi \in \mathbb{R}^{256 \times 512}$). These results are from fully linear VAEs (both the encoder and decoder were linear). Features are ordered from top-left to bottom-right, in ascending order of their associated KL divergence (\mathcal{P} -VAE, \mathcal{G} -VAE, \mathcal{L} -VAE), or the magnitude of posterior logits (\mathcal{C} -VAE). The sparse coding results (LCA and ISTA) are ordered randomly.

cortical neurons [3]. Inspecting the dictionaries learned by different models demonstrates this is not trivial (Fig. 2). As expected from theoretical results [4], \mathcal{G} -VAE (top left) learn probabilistic PCA, but with many noisy elements. As demonstrated previously [40, 90], \mathcal{L} -VAE (lower left) learn Gabor-like elements. However, there are a large number of noisy basis vectors. It is of note that previous work did not show complete dictionaries for their results with Laplace priors [40, 90]. In contrast, \mathcal{P} -VAE (top middle) learns Gabor-like filters that cover space, orientation, and spatial frequency. The quality is comparable to sparse coding dictionaries learned with LCA/ISTA (top/lower right panels). \mathcal{C} -VAE also learns Gabor filters, although there are significantly more noisy basis elements.

The \mathcal{P} -VAE avoids posterior collapse. A striking feature of Fig. 2 is the sheer number of noisy basis vectors for both continuous VAEs (\mathcal{G} -VAE, \mathcal{L} -VAE). We suspected this reflected dead neurons with vanishing KL, which is indicative of a collapsed latent dimension that's no longer encoding information. To quantify this, we binned the distribution of KL values and thresholded the resulting distribution at discontinuous points (see supplemental Fig. 5). Table 2 shows the results of this analysis for all VAEs with valid KL terms. Across all datasets, both continuous VAEs suffered from large numbers of dead neurons, whereas \mathcal{P} -VAE largely avoided this problem. On both natural image datasets, \mathcal{P} -VAE had $\sim 2\%$ dead neurons compared to $\sim 80\%$ for \mathcal{G} -VAE and \mathcal{L} -VAE. Having a more expressive encoder slightly increases this percentage, but a dramatic difference between \mathcal{P} -VAE and continuous VAEs (\mathcal{G} -VAE, \mathcal{L} -VAE) persists.

Table 2: Proportion of active neurons. All models considered in this table had a latent dimensionality of $K = 512$. The decoders were linear, and the encoders were either linear or convolutional.

Model	van Hateren		CIFAR $_{16 \times 16}$		MNIST	
	linear	conv	linear	conv	linear	conv
\mathcal{P} -VAE	0.984 \pm .011	0.819 \pm .041	0.999 \pm .002	0.928 \pm .045	0.537 \pm .008	0.426 \pm .011
\mathcal{L} -VAE	0.188 \pm .000	0.222 \pm .003	0.193 \pm .003	0.230 \pm .000	0.027 \pm .000	0.034 \pm .002
\mathcal{G} -VAE	0.218 \pm .003	0.246 \pm .000	0.105 \pm .008	0.246 \pm .000	0.027 \pm .000	0.031 \pm .000

The \mathcal{P} -VAE learns sparse representations. To quantify whether \mathcal{P} -VAE learns sparse representations, we compared our VAE models to sparse coding trained with LCA and ISTA and quantified the lifetime sparsity [68]. The lifetime sparsity of the j -th latent is:

$$s_j = \left(1 - \frac{1}{N} \frac{(\sum_i z_{ij})^2}{\sum_i z_{ij}^2} \right) \Bigg/ \left(1 - \frac{1}{N} \right), \quad (5)$$

where N is the number of images, and z_{ij} is sampled from the posterior for the i -th image. Intuitively, $s_j = 1$ whenever neuron j responds to a single stimulus out of the entire set (highly selective). In contrast, $s_j = 0$ whenever the neuron responds equally well to all stimuli indiscriminately.

Fig. 3a shows the reconstruction performance (MSE) compared to lifetime sparsity (s , eq. (5)) for all VAEs. The \mathcal{G} -VAE finds good reconstructions (MSE = 71.49) but with low sparsity ($s = 0.37$). The \mathcal{P} -VAE finds much sparser solutions ($s = 0.94$), but at a cost of reconstruction quality (MSE = 102.68). Because the \mathcal{P} -VAE KL term explicitly penalizes rate (eq. (3)), we explored different β values for \mathcal{P} -VAE with a linear encoder and decoder (Fig. 3a, blue curve). This maps out a rate-distortion curve, allowing us to compare what level of sparsity \mathcal{P} -VAE matches \mathcal{G} -VAE performance. Even with a simpler (linear) encoder, \mathcal{P} -VAE matches \mathcal{G} -VAE in performance with a $1.6 \times$ sparser solution (at $\beta = 0.6$). The addition of a relu activation to \mathcal{G} -VAE increased the sparsity ($s = 0.69$). By comparing the \mathcal{P} -VAE with a linear encoder to \mathcal{P} -VAE with a convolutional encoder, we find that increasing decoder complexity for the same $\beta = 1$ maintains the same MSE but increases sparsity (blue open circle), suggesting amortization quality can significantly shift this curve [33, 106, 107]¹.

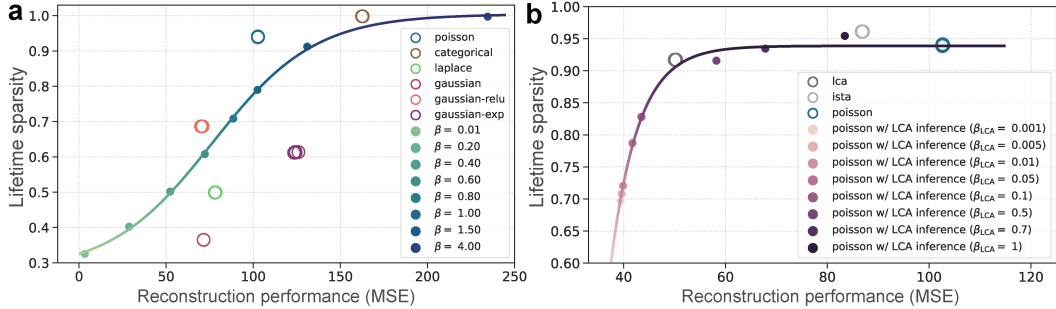


Figure 3: Reconstruction performance versus sparsity of representations. (a) Results for VAE model family. The curve is sigmoid fit to a \mathcal{P} -VAE with both linear encoder and decoder, and varying β values (this is β from eq. (4)). (b) Amortization gap of \mathcal{P} -VAE (blue open circle) compared to sparse coding (LCA/ISTA). Solid points are obtained from LCA inference applied to the \mathcal{P} -VAE basis vectors with different sparsity levels (β_{LCA} is the one from eq. (1)). The curve is a sigmoid fit.

Does \mathcal{P} -VAE match the performance of traditional sparse coding trained with LCA or ISTA? Figure 3b compares \mathcal{P} -VAE to sparse coding models that were trained using a wide range of hyperparameters, and the best models were selected for each class (appendix A). \mathcal{P} -VAE achieves a similar sparsity to LCA and ISTA ($s = 0.94, 0.91$, and 0.96 , respectively), but the best LCA model drastically outperforms \mathcal{P} -VAE on MSE for similar levels of sparsity. This suggests our convolutional encoder is struggling to close the amortization gap. To test this hypothesis, we performed LCA inference on basis elements learned by \mathcal{P} -VAE (Fig. 3b curve/solid points). We explored a range of hyperparameters to determine whether the MSE improved for similar sparsity levels. Indeed, LCA inference using \mathcal{P} -VAE dictionary, was able to nearly match the performance of sparse coding LCA for similar levels of sparsity. This confirms our hypothesis that a large amortization gap remains for the specific encoder architectures we tested, highlighting the need for improved inference algorithms/architectures [107].

The \mathcal{P} -VAE is more sample efficient in downstream tasks. We test the unsupervised learned representations on a downstream classification task. We first trained all VAE models with $K = 10$ dimensional latent space and a convolutional encoder and decoder on the MNIST training set (see supplementary Fig. 6 for the quality of generated samples and reconstruction performance). Next, we used the trained encoders to extract representations and evaluated their performance on classifying MNIST digits. We define VAE representation to be the output of the encoder. Following conventions in the VAE literature [104], we used the mean vectors μ for continuous VAEs (\mathcal{G} -VAE, \mathcal{L} -VAE). For the \mathcal{P} -VAE, we used $\log \delta r$, and for the \mathcal{C} -VAE, we used logits.

We split the MNIST validation set into two 5,000 sample sets, used as train/test sets for this task. We train a K-nearest neighbors (KNN) classifier with a varying number of limited supervised samples ($N = 200, 1000, 5000$) drawn without replacement from the first set (train), to measure classification

¹Due to the computational complexity of \mathcal{P} -VAE with convolutional encoder, we were not able to sweep out a full β -dependent curve before this submission, but will do for the final.

Table 3: Geometry of representations ($K = 10$ only; see Table 5 for the full set of results).

Latent dim.	Model	KNN classification (N , # labeled samples)			Shattering dim.
		$N = 200$	$N = 1,000$	$N = 5,000$	
$K = 10$	\mathcal{P} -VAE	0.815 \pm .002	0.919 \pm .001	0.946 \pm .017	0.797 \pm .009
	\mathcal{C} -VAE	0.705 \pm .002	0.800 \pm .002	0.853 \pm .040	0.795 \pm .006
	\mathcal{L} -VAE	0.757 \pm .003	0.869 \pm .002	0.924 \pm .028	0.751 \pm .008
	\mathcal{G} -VAE	0.673 \pm .003	0.813 \pm .002	0.891 \pm .033	0.758 \pm .007
	\mathcal{G} -VAE _{relu}	0.694 \pm .003	0.817 \pm .003	0.877 \pm .045	0.762 \pm .007
	\mathcal{G} -VAE _{exp}	0.642 \pm .003	0.784 \pm .002	0.863 \pm .032	0.737 \pm .008

accuracy on the withheld set (test). KNN is nonparametric, and its performance is directly influenced by the geometry of representations by explicitly capturing the distance between encoded samples [108]. We find that using only $N = 200$ samples, \mathcal{P} -VAE achieves $\sim 82\%$ accuracy in held out data; whereas, \mathcal{G} -VAE achieves the same level of accuracy at $N = 1000$ samples (Table 3). By this measure, \mathcal{P} -VAE is $5\times$ more sample efficient. But from Alleman et al. [109], we know that the choice of activation function changes the geometry of learned representations. Therefore, we also tested \mathcal{G} -VAE models with an activation function (relu and exp) applied to latents after sampling from the posterior. This biological constraint improved \mathcal{G} -VAE, but it still underperformed \mathcal{P} -VAE (Table 3). We also found this result held for higher dimensional latent spaces (supplementary Table 5).

The \mathcal{P} -VAE learns representations with higher dimensional geometry. The preceding results are indicative of substantial differences in the geometry of the representations learned by \mathcal{P} -VAE compared to other VAE families (Table 3). To test this more explicitly, we calculated the “shattering dimensionality” of the latent space [110–112]. Shattering dim measures the average accuracy over all possible pairwise classification tasks. This is called “shattering” because if the model shatters data points around into a high dimensional space, they will become more linearly separable. For MNIST with 10 classes, there are $\binom{10}{5} = 252$ possible classifications. We trained logistic regression on the entire training set to classify each of the 252 arbitrary splits and measured the average performance on the entire validation set. The far right column of Table 3 shows the measured shattering dims. For $K = 10$, the shattering dim was significantly higher for discrete VAEs (\mathcal{P} -VAE, \mathcal{C} -VAE). For higher dimensional latent spaces \mathcal{P} -VAE strongly outperformed alternative models (Table 5).

5 Conclusions

In this paper, we describe the \mathcal{P} -VAE, which performs posterior inference encoded in discrete spike counts. We introduce a Poisson reparameterization trick and derive the ELBO for Poisson-distributed VAEs. The \mathcal{P} -VAE loss results in a KL term that penalizes firing rates like sparse coding [3]. We show that \mathcal{P} -VAE with a linear generative model reduces to amortized sparse coding.

When trained on natural image patches, \mathcal{P} -VAE with a linear decoder learns sparse solutions with Gabor-like basis vectors resembling sparse coding, both in the form of the learned basis as well as the lifetime sparsity of the latents. We evaluated the representations on downstream classification tasks and found that \mathcal{P} -VAE encodes its inputs in a higher dimensional space that enabled good linear separability between classes.

Limitations and future directions. \mathcal{P} -VAE samples latents that are conditionally Poisson. Although this is inspired by the statistics of spike counts in the brain over short time intervals [50], there are deviations from Poisson throughout the cortex over longer time windows [51]. Extending \mathcal{P} -VAE to hierarchical architectures [33] will make the latents conditionally Poisson, but not marginally Poisson (as they are modulated by top-down rates). Further extensions could implement doubly-stochastic spike generation [51, 113]. A second limitation is the amortization gap we observed between our current implementation of \mathcal{P} -VAE and traditional sparse coding. This could likely be closed with more expressive encoders [114], but it is an open area of research [107].

Overall, the \mathcal{P} -VAE is a promising step towards learning brain-like representations in deep hierarchical generative models.

References

- [1] Irina Higgins et al. “Unsupervised deep learning identifies semantic disentanglement in single inferotemporal face patch neurons”. In: *Nature Communications* 12.1 (2021), p. 6456. DOI: 10.1038/s41467-021-26751-5.
- [2] Hadi Vafaii et al. “Hierarchical VAEs provide a normative account of motion processing in the primate brain”. In: *Thirty-seventh Conference on Neural Information Processing Systems*. 2023. URL: <https://openreview.net/forum?id=1w0kHN9JK8>.
- [3] Bruno A Olshausen and David J Field. “Emergence of simple-cell receptive field properties by learning a sparse code for natural images”. In: *Nature* 381.6583 (1996), pp. 607–609. DOI: 10.1038/381607a0.
- [4] Michael E. Tipping and Christopher M. Bishop. “Probabilistic Principal Component Analysis”. In: *Journal of the Royal Statistical Society Series B: Statistical Methodology* 61.3 (Jan. 1999), pp. 611–622. ISSN: 1369-7412. DOI: 10.1111/1467-9868.00196.
- [5] Warren S McCulloch and Walter Pitts. “A logical calculus of the ideas immanent in nervous activity”. In: *The bulletin of mathematical biophysics* 5 (1943), pp. 115–133. DOI: 10.1007/BF02478259.
- [6] Patricia S Churchland and Terrence J Sejnowski. “Perspectives on cognitive neuroscience”. In: *Science* 242.4879 (1988), pp. 741–745. DOI: 10.1126/science.3055294.
- [7] Michael SC Thomas and James L McClelland. “Connectionist models of cognition”. In: *The Cambridge handbook of computational psychology* (2008), pp. 23–58. URL: <http://www7.bbk.ac.uk/psychology/dnl/wp-content/uploads/2023/10/Thomas-McClelland-proof.pdf>.
- [8] Nikolaus Kriegeskorte. “Deep neural networks: a new framework for modeling biological vision and brain information processing”. In: *Annual Review of Vision Science* 1 (2015), pp. 417–446. DOI: 10.1101/029876.
- [9] Grace W. Lindsay. “Convolutional Neural Networks as a Model of the Visual System: Past, Present, and Future”. In: *Journal of Cognitive Neuroscience* 33.10 (Sept. 2021), pp. 2017–2031. ISSN: 0898-929X. DOI: 10.1162/jocn_a_01544.
- [10] Joseph Marino. “Predictive coding, variational autoencoders, and biological connections”. In: *Neural Computation* 34.1 (2022), pp. 1–44. DOI: 10.1162/neco_a_01458.
- [11] Jeffrey S Bowers et al. “Deep problems with neural network models of human vision”. In: *Behavioral and Brain Sciences* 46 (2023), e385. DOI: 10.1017/S0140525X22002813.
- [12] Felix A. Wichmann and Robert Geirhos. “Are Deep Neural Networks Adequate Behavioral Models of Human Visual Perception?” In: *Annual Review of Vision Science* 9. Volume 9, 2023 (2023), pp. 501–524. ISSN: 2374-4650. DOI: 10.1146/annurev-vision-120522-031739.
- [13] Anthony Zador et al. “Catalyzing next-generation Artificial Intelligence through NeuroAI”. In: *Nature Communications* 14.1 (2023), p. 1597. DOI: 10.1038/s41467-023-37180-x.
- [14] Fabian H Sinz et al. “Engineering a less artificial intelligence”. In: *Neuron* 103.6 (2019), pp. 967–979. DOI: 10.1016/j.neuron.2019.08.034.
- [15] Demis Hassabis et al. “Neuroscience-inspired artificial intelligence”. In: *Neuron* 95.2 (2017), pp. 245–258. DOI: 10.1016/j.neuron.2017.06.011.
- [16] Nancy Kanwisher et al. “Using artificial neural networks to ask ‘why’ questions of minds and brains”. In: *Trends in Neurosciences* (2023). DOI: 10.1016/j.tins.2022.12.008.
- [17] Blake Richards et al. “The application of artificial intelligence to biology and neuroscience”. In: *Cell* 185.15 (2022), pp. 2640–2643. DOI: 10.1016/j.cell.2022.06.047.
- [18] Blake A Richards et al. “A deep learning framework for neuroscience”. In: *Nature Neuroscience* 22.11 (2019), pp. 1761–1770. DOI: 10.1038/s41593-019-0520-2.
- [19] David GT Barrett et al. “Analyzing biological and artificial neural networks: challenges with opportunities for synergy?” In: *Current Opinion in Neurobiology* 55 (2019), pp. 55–64. DOI: 10.1016/j.conb.2019.01.007.
- [20] Adrien Doerig et al. “The neuroconnectionist research programme”. In: *Nature Reviews Neuroscience* (2023), pp. 1–20. DOI: 10.1038/s41583-023-00705-w.
- [21] Ibn al-Haytham. *Book of optics (Kitab Al-Manazir)*. 1011–1021 AD.
- [22] Hermann Von Helmholtz. *Handbuch der physiologischen Optik*. Vol. 9. Voss, 1867.

[23] Tai Sing Lee and David Mumford. “Hierarchical Bayesian inference in the visual cortex”. In: *JOSA A* 20.7 (2003), pp. 1434–1448. DOI: 10.1364/JOSAA.20.001434.

[24] Bruno A. Olshausen. “Perception as an Inference Problem”. In: *The Cognitive Neurosciences (5th edition)* (2014). Ed. by Michael Gazzaniga and George R. Mangun. DOI: 10.7551/mitpress/9504.003.0037. URL: <http://rctn.org/bruno/papers/perception-as-inference.pdf>.

[25] Edwin Garrigues Boring. “Perception of objects”. In: *American Journal of Physics* (1946). DOI: 10.1119/1.1990807.

[26] Karl Friston. “The free-energy principle: a unified brain theory?” In: *Nature Reviews Neuroscience* 11.2 (2010), pp. 127–138. DOI: 10.1038/nrn2787.

[27] Sam Bond-Taylor et al. “Deep generative modelling: A comparative review of vaes, gans, normalizing flows, energy-based and autoregressive models”. In: *IEEE transactions on pattern analysis and machine intelligence* 44.11 (2021), pp. 7327–7347. DOI: 10.1109/TPAMI.2021.3116668.

[28] Stanley H. Chan. *Tutorial on Diffusion Models for Imaging and Vision*. 2024. arXiv: 2403.18103 [cs.LG].

[29] Wayne Xin Zhao et al. *A Survey of Large Language Models*. 2023. arXiv: 2303.18223 [cs.CL].

[30] Rajesh PN Rao and Dana H Ballard. “Predictive coding in the visual cortex: a functional interpretation of some extra-classical receptive-field effects”. In: *Nature Neuroscience* 2.1 (1999), pp. 79–87. DOI: 10.1038/4580.

[31] Robin Rombach et al. “High-Resolution Image Synthesis With Latent Diffusion Models”. In: *Proceedings of the IEEE/CVF Conference on Computer Vision and Pattern Recognition (CVPR)*. June 2022, pp. 10684–10695.

[32] Tero Karras et al. “A Style-Based Generator Architecture for Generative Adversarial Networks”. In: *Proceedings of the IEEE/CVF Conference on Computer Vision and Pattern Recognition (CVPR)*. June 2019. URL: https://openaccess.thecvf.com/content_CVPR_2019/html/Karras_A_Style-Based_Generator_Architecture_for_Generative_Adversarial_Networks_CVPR_2019_paper.html.

[33] Arash Vahdat and Jan Kautz. “NVAE: A Deep Hierarchical Variational Autoencoder”. In: *Advances in Neural Information Processing Systems*. Vol. 33. Curran Associates, Inc., 2020, pp. 19667–19679. URL: https://papers.nips.cc/paper_files/paper/2020/hash/e3b21256183cf7c2c7a66be163579d37-Abstract.html.

[34] Rewon Child. “Very Deep {VAE}s Generalize Autoregressive Models and Can Outperform Them on Images”. In: *International Conference on Learning Representations*. 2021. URL: <https://openreview.net/forum?id=RLRXCV6DbEJ>.

[35] Diederik P Kingma and Max Welling. “Auto-encoding variational bayes”. In: (2014). arXiv: 1312.6114v11 [stat.ML].

[36] Danilo Jimenez Rezende et al. “Stochastic backpropagation and approximate inference in deep generative models”. In: *International Conference on Machine Learning*. PMLR. 2014, pp. 1278–1286. URL: <https://proceedings.mlr.press/v32/rezende14.html>.

[37] Diederik P Kingma and Ruizhi Gao. “Understanding Diffusion Objectives as the ELBO with Simple Data Augmentation”. In: *Thirty-seventh Conference on Neural Information Processing Systems*. 2023. URL: <https://openreview.net/forum?id=NnMEadcdyD>.

[38] Karsten Kreis et al. *NeurIPS 2023 Tutorial on Latent Diffusion Models*. <https://neurips2023-1dm-tutorial.github.io/>. 2023.

[39] Diederik Kingma et al. “Variational diffusion models”. In: *Advances in neural information processing systems* 34 (2021), pp. 21696–21707.

[40] Ferenc Csikor et al. “Top-down perceptual inference shaping the activity of early visual cortex”. In: *bioRxiv* (2023). DOI: 10.1101/2023.11.29.569262.

[41] T. Anderson Keller et al. “Modeling Category-Selective Cortical Regions with Topographic Variational Autoencoders”. In: *SVRHM 2021 Workshop @ NeurIPS*. 2021. URL: https://openreview.net/forum?id=yGRq_1W54bI.

[42] T. Anderson Keller and Max Welling. “Topographic VAEs learn Equivariant Capsules”. In: *Advances in Neural Information Processing Systems*. Ed. by M. Ranzato et al. Vol. 34. Curran Associates, Inc., 2021, pp. 28585–28597. URL: <https://proceedings.neurips.cc/paper/2021/hash/f03704cb51f02f80b09bfffba15751691-Abstract.html>.

[43] Katherine R Storrs et al. “Unsupervised learning predicts human perception and misperception of gloss”. In: *Nature Human Behaviour* 5.10 (2021), pp. 1402–1417. DOI: 10.1038/s41562-021-01097-6.

[44] Edgar Adrian. *The activity of the nerve fibres*. <https://www.nobelprize.org/prizes/medicine/1932/adrian/lecture/>. 1932.

[45] Edgar Douglas Adrian and Yngve Zotterman. “The impulses produced by sensory nerve-endings: Part II. The response of a Single End-Organ”. In: *The Journal of Physiology* (1926), pp. 151–71. DOI: 10.1113/jphysiol.1926.sp002281.

[46] Donald H Perkel and Theodore H Bullock. “Neural coding”. In: *Neurosciences Research Program Bulletin* (1968). URL: <https://ntrs.nasa.gov/citations/19690022317>.

[47] Horace B Barlow. “Single units and sensation: a neuron doctrine for perceptual psychology?” In: *Perception* 1.4 (1972), pp. 371–394. DOI: 10.1088/p010371.

[48] Ehud Zohary et al. “Correlated neuronal discharge rate and its implications for psychophysical performance”. In: *Nature* 370.6485 (1994), pp. 140–143. DOI: 10.1038/370140a0.

[49] Fred Rieke et al. *Spikes: exploring the neural code*. MIT press, 1999.

[50] Malvin C Teich. “Fractal character of the auditory neural spike train”. In: *IEEE Transactions on Biomedical Engineering* 36.1 (1989), pp. 150–160.

[51] Robbe LT Goris et al. “Partitioning neuronal variability”. In: *Nature neuroscience* 17.6 (2014), pp. 858–865.

[52] Diederik P Kingma and Max Welling. “An introduction to variational autoencoders”. In: *Foundations and Trends® in Machine Learning* 12.4 (2019), pp. 307–392. DOI: 10.1561/2200000056.

[53] Charles D Gilbert and Wu Li. “Top-down influences on visual processing”. In: *Nature Reviews Neuroscience* 14.5 (2013), pp. 350–363.

[54] David C Knill and Alexandre Pouget. “The Bayesian brain: the role of uncertainty in neural coding and computation”. In: *Trends in Neurosciences* 27.12 (2004), pp. 712–719. DOI: 10.1016/j.tins.2004.10.007.

[55] Karl Friston. “The free-energy principle: a rough guide to the brain?” In: *Trends in cognitive sciences* 13.7 (2009), pp. 293–301.

[56] Peter Dayan et al. “The Helmholtz machine”. In: *Neural Computation* 7.5 (1995), pp. 889–904. DOI: 10.1162/neco.1995.7.5.889.

[57] William Lotter et al. “Deep Predictive Coding Networks for Video Prediction and Unsupervised Learning”. In: *International Conference on Learning Representations*. 2017. URL: <https://openreview.net/forum?id=B1ewdt9xe>.

[58] Fred Attneave. “Some informational aspects of visual perception.” In: *Psychological review* 61.3 (1954), p. 183.

[59] Horace B Barlow et al. “Possible principles underlying the transformation of sensory messages”. In: *Sensory communication* 1.01 (1961), pp. 217–233.

[60] Mandyam Veerambudi Srinivasan et al. “Predictive coding: a fresh view of inhibition in the retina”. In: *Proceedings of the Royal Society of London. Series B. Biological Sciences* 216.1205 (1982), pp. 427–459. DOI: 10.1098/rspb.1982.0085.

[61] Karl Friston. “A theory of cortical responses”. In: *Philosophical transactions of the Royal Society B: Biological Sciences* 360.1456 (2005), pp. 815–836. DOI: 10.1098/rstb.2005.1622.

[62] Andy Clark. “Whatever next? Predictive brains, situated agents, and the future of cognitive science”. In: *Behavioral and brain sciences* 36.3 (2013), pp. 181–204. DOI: 10.1017/S0140525X12000477.

[63] William Lotter et al. “A neural network trained for prediction mimics diverse features of biological neurons and perception”. In: *Nature machine intelligence* 2.4 (2020), pp. 210–219. DOI: 10.1038/s42256-020-0170-9.

[64] Beren Millidge et al. “Predictive coding networks for temporal prediction”. In: *PLOS Computational Biology* 20.4 (2024), e1011183.

[65] Yosef Singer et al. “Hierarchical temporal prediction captures motion processing along the visual pathway”. In: *Elife* 12 (2023), e52599.

[66] Pierre-Étienne Fiquet and Eero Simoncelli. “A polar prediction model for learning to represent visual transformations”. In: *Advances in Neural Information Processing Systems* 36 (2024).

[67] Bruno A Olshausen and David J Field. “Sparse coding of sensory inputs”. In: *Current opinion in neurobiology* 14.4 (2004), pp. 481–487. DOI: 10.1016/j.conb.2004.07.007.

[68] William E Vinje and Jack L Gallant. “Sparse coding and decorrelation in primary visual cortex during natural vision”. In: *Science* 287.5456 (2000), pp. 1273–1276. DOI: 10.1126/science.287.5456.1273.

[69] Alison L Barth and James FA Poulet. “Experimental evidence for sparse firing in the neocortex”. In: *Trends in neurosciences* 35.6 (2012), pp. 345–355. DOI: 10.1016/j.tins.2012.03.008.

[70] R Quijan Quiroga et al. “Sparse but not ‘grandmother-cell’ coding in the medial temporal lobe”. In: *Trends in cognitive sciences* 12.3 (2008), pp. 87–91. DOI: 10.1016/j.tics.2007.12.003.

[71] Tomáš Hromádka et al. “Sparse representation of sounds in the unanesthetized auditory cortex”. In: *PLoS biology* 6.1 (2008), e16. DOI: 10.1371/journal.pbio.0060016.

[72] Cindy Poo and Jeffry S Isaacson. “Odor representations in olfactory cortex: “sparse” coding, global inhibition, and oscillations”. In: *Neuron* 62.6 (2009), pp. 850–861. DOI: 10.1016/j.neuron.2009.05.022.

[73] Jason Wolfe et al. “Sparse and powerful cortical spikes”. In: *Current opinion in neurobiology* 20.3 (2010), pp. 306–312. DOI: 10.1016/j.conb.2010.03.006.

[74] Ben DB Willmore et al. “Sparse coding in striate and extrastriate visual cortex”. In: *Journal of neurophysiology* 105.6 (2011), pp. 2907–2919. DOI: 10.1152/jn.00594.2010.

[75] Bilal Haider et al. “Synaptic and network mechanisms of sparse and reliable visual cortical activity during nonclassical receptive field stimulation”. In: *Neuron* 65.1 (2010), pp. 107–121. DOI: 10.1016/j.neuron.2009.12.005.

[76] Sylvain Crochet et al. “Synaptic mechanisms underlying sparse coding of active touch”. In: *Neuron* 69.6 (2011), pp. 1160–1175. DOI: 10.1016/j.neuron.2011.02.022.

[77] Carl CH Petersen. “Sensorimotor processing in the rodent barrel cortex”. In: *Nature Reviews Neuroscience* 20.9 (2019), pp. 533–546. DOI: 10.1038/s41583-019-0200-y.

[78] Emmanouil Froudarakis et al. “Population code in mouse V1 facilitates readout of natural scenes through increased sparseness”. In: *Nature neuroscience* 17.6 (2014), pp. 851–857. DOI: 10.1038/nn.3707.

[79] Christopher J Rozell et al. “Sparse coding via thresholding and local competition in neural circuits”. In: *Neural Computation* 20.10 (2008), pp. 2526–2563. DOI: 10.1162/neco.2008.03-07-486.

[80] I. Daubechies et al. “An iterative thresholding algorithm for linear inverse problems with a sparsity constraint”. In: *Communications on Pure and Applied Mathematics* 57.11 (2004), pp. 1413–1457. DOI: 10.1002/cpa.20042.

[81] Amir Beck and Marc Teboulle. “A Fast Iterative Shrinkage-Thresholding Algorithm for Linear Inverse Problems”. In: *SIAM Journal on Imaging Sciences* 2.1 (2009), pp. 183–202. DOI: 10.1137/080716542.

[82] Ankush Ganguly et al. “Amortized Variational Inference: A Systematic Review”. In: *Journal of Artificial Intelligence Research* 78 (2023), pp. 167–215. DOI: 10.1613/jair.1.14258.

[83] Brandon Amos. “Tutorial on Amortized Optimization”. In: *Foundations and Trends® in Machine Learning* 16.5 (2023), pp. 592–732. ISSN: 1935-8237. DOI: 10.1561/2200000102.

[84] Samuel Gershman and Noah Goodman. “Amortized inference in probabilistic reasoning”. In: *Proceedings of the annual meeting of the cognitive science society*. Vol. 36. 36. 2014. URL: <https://escholarship.org/uc/item/34j1h7k5>.

[85] Colin Conwell et al. “What can 1.8 billion regressions tell us about the pressures shaping high-level visual representation in brains and machines?” In: *bioRxiv* (2023). DOI: 10.1101/2022.03.28.485868.

[86] Eric Elmoznino and Michael F Bonner. “High-performing neural network models of visual cortex benefit from high latent dimensionality”. In: *bioRxiv* (2022), pp. 2022–07. DOI: 10.1101/2022.07.13.499969.

[87] Aaron Van Den Oord, Oriol Vinyals, et al. “Neural discrete representation learning”. In: *Advances in neural information processing systems* 30 (2017).

[88] Eric Jang et al. “Categorical Reparameterization with Gumbel-Softmax”. In: *International Conference on Learning Representations*. 2017. URL: <https://openreview.net/forum?id=rkE3y85ee>.

[89] Hiromichi Kamata et al. “Fully spiking variational autoencoder”. In: *Proceedings of the AAAI Conference on Artificial Intelligence*. Vol. 36. 6. 2022, pp. 7059–7067.

[90] Victor Geadah et al. “Sparse-Coding Variational Auto-Encoders”. In: *bioRxiv* (2024). DOI: 10.1101/399246.

[91] Francesco Tonolini et al. “Variational sparse coding”. In: *Uncertainty in Artificial Intelligence*. PMLR. 2020, pp. 690–700.

[92] Pan Xiao et al. “SC-VAE: Sparse Coding-based Variational Autoencoder with Learned ISTA”. In: (2024). arXiv: 2303.16666 [cs.CV].

[93] David Roxbee Cox and Valerie Isham. *Point processes*. Vol. 12. CRC Press, 1980.

[94] Oleksandr Shchur et al. “Fast and Flexible Temporal Point Processes with Triangular Maps”. In: *Advances in Neural Information Processing Systems*. Ed. by H. Larochelle et al. Vol. 33. Curran Associates, Inc., 2020, pp. 73–84. URL: https://proceedings.neurips.cc/paper_files/paper/2020/hash/00ac8ed3b4327bdd4ebbebcb2ba10a00-Abstract.html.

[95] Oleksandr Shchur. “Modeling Continuous-time Event Data with Neural Temporal Point Processes”. PhD thesis. Technische Universität München, 2022.

[96] Adam Paszke et al. “PyTorch: An Imperative Style, High-Performance Deep Learning Library”. In: *Advances in Neural Information Processing Systems*. Vol. 32. Curran Associates, Inc., 2019. URL: https://papers.nips.cc/paper_2019/hash/bdbca288fee7f92f2bfa9f7012727740-Abstract.html.

[97] Chris J. Maddison et al. “The Concrete Distribution: A Continuous Relaxation of Discrete Random Variables”. In: *International Conference on Learning Representations*. 2017. URL: <https://openreview.net/forum?id=S1jE5L5g1>.

[98] Daniel J Felleman and David C Van Essen. “Distributed hierarchical processing in the primate cerebral cortex”. In: *Cerebral Cortex* 1.1 (1991), pp. 1–47. DOI: 10.1093/CERCOR/1.1.1.

[99] Anita A Disney. “Neuromodulatory control of early visual processing in macaque”. In: *Annual Review of Vision Science* 7 (2021), pp. 181–199.

[100] James C. R. Whittington et al. “Disentanglement with Biological Constraints: A Theory of Functional Cell Types”. In: *The Eleventh International Conference on Learning Representations*. 2023. URL: https://openreview.net/forum?id=9Z_GfhZnGH.

[101] J Hans Van Hateren and Arjen van der Schaaf. “Independent component filters of natural images compared with simple cells in primary visual cortex”. In: *Proceedings of the Royal Society of London. Series B: Biological Sciences* 265.1394 (1998), pp. 359–366.

[102] Victor Boutin et al. “Sparse deep predictive coding captures contour integration capabilities of the early visual system”. In: *PLoS computational biology* 17.1 (2021), e1008629.

[103] Alex Krizhevsky, Geoffrey Hinton, et al. “Learning multiple layers of features from tiny images”. In: (2009).

[104] Francesco Locatello et al. “Challenging common assumptions in the unsupervised learning of disentangled representations”. In: *international conference on machine learning*. PMLR. 2019, pp. 4114–4124. URL: <https://proceedings.mlr.press/v97/locatello19a.html>.

[105] Yoshua Bengio et al. “Estimating or Propagating Gradients Through Stochastic Neurons for Conditional Computation”. In: (2013). arXiv: 1308.3432 [cs.LG].

[106] Alexander Alemi et al. “Fixing a Broken ELBO”. In: *Proceedings of the 35th International Conference on Machine Learning*. Ed. by Jennifer Dy and Andreas Krause. Vol. 80. Proceedings of Machine Learning Research. PMLR, July 2018, pp. 159–168. URL: <https://proceedings.mlr.press/v80/alemi18a.html>.

[107] Chris Cremer et al. “Inference suboptimality in variational autoencoders”. In: *International Conference on Machine Learning*. PMLR. 2018, pp. 1078–1086.

[108] Kilian Q Weinberger and Lawrence K Saul. “Distance metric learning for large margin nearest neighbor classification.” In: *Journal of machine learning research* 10.2 (2009).

[109] Matteo Alleman et al. “Task structure and nonlinearity jointly determine learned representational geometry”. In: *The Twelfth International Conference on Learning Representations*. 2024. URL: <https://openreview.net/forum?id=k9t8dQ30kU>.

[110] Mattia Rigotti et al. “The importance of mixed selectivity in complex cognitive tasks”. In: *Nature* 497.7451 (2013), pp. 585–590. DOI: 10.1038/nature12160.

[111] Silvia Bernardi et al. “The geometry of abstraction in the hippocampus and prefrontal cortex”. In: *Cell* 183.4 (2020), pp. 954–967.

[112] Matthew T Kaufman et al. “The implications of categorical and category-free mixed selectivity on representational geometries”. In: *Current opinion in neurobiology* 77 (2022), p. 102644.

[113] Cina Aghamohammadi et al. “A doubly stochastic renewal framework for partitioning spiking variability”. In: *bioRxiv* (2024), pp. 2024–02.

[114] Karol Gregor and Yann LeCun. “Learning fast approximations of sparse coding”. In: *Proceedings of the 27th international conference on international conference on machine learning*. 2010, pp. 399–406.

[115] Ashish Vaswani et al. “Attention is All you Need”. In: *Advances in Neural Information Processing Systems*. Ed. by I. Guyon et al. Vol. 30. Curran Associates, Inc., 2017. URL: https://papers.nips.cc/paper_files/paper/2017/hash/3f5ee243547dee91fdb053c1c4a845aa-Abstract.html.

[116] Prajit Ramachandran et al. “Searching for Activation Functions”. In: *International Conference on Learning Representations*. 2018. URL: <https://openreview.net/forum?id=SkBYYyZRZ>.

[117] Stefan Elfwing et al. “Sigmoid-weighted linear units for neural network function approximation in reinforcement learning”. In: *Neural Networks* 107 (2018), pp. 3–11. DOI: 10.1016/j.neunet.2017.12.012.

[118] Diederik P Kingma and Jimmy Ba. “Adam: A method for stochastic optimization”. In: (2014). arXiv: 1412.6980 [cs.LG].

[119] Ilya Loshchilov and Frank Hutter. “SGDR: Stochastic Gradient Descent with Warm Restarts”. In: *International Conference on Learning Representations*. 2017. URL: <https://openreview.net/forum?id=Skq89Scxx>.

[120] Casper Kaae Sønderby et al. “Ladder Variational Autoencoders”. In: *Advances in Neural Information Processing Systems*. Vol. 29. Curran Associates, Inc., 2016. URL: https://papers.nips.cc/paper_files/paper/2016/hash/6ae07dcb33ec3b7c814df797cbda0f87-Abstract.html.

[121] Samuel R. Bowman et al. “Generating Sentences from a Continuous Space”. In: *Proceedings of the 20th SIGNLL Conference on Computational Natural Language Learning*. Berlin, Germany: Association for Computational Linguistics, Aug. 2016, pp. 10–21. DOI: 10.18653/v1/K16-1002.

[122] Hao Fu et al. “Cyclical Annealing Schedule: A Simple Approach to Mitigating KL Vanishing”. In: *Proceedings of the 2019 Conference of the North American Chapter of the Association for Computational Linguistics: Human Language Technologies, Volume 1 (Long and Short Papers)*. Minneapolis, Minnesota: Association for Computational Linguistics, June 2019, pp. 240–250. DOI: 10.18653/v1/N19-1021.

[123] Shakir Mohamed et al. “Monte Carlo Gradient Estimation in Machine Learning”. In: *Journal of Machine Learning Research* 21.132 (2020), pp. 1–62. URL: <http://jmlr.org/papers/v21/19-346.html>.

A Architecture, training, and hyperparameter details

A.1 Datasets: additional details

We consider three datasets in this paper. We tile up the van Hateren dataset of natural images [101] and CIFAR10 into 16×16 patches and apply whitening and contrast normalization using the code made available by Boutin et al. [102]. This operation results in the following total number of samples:

- **van Hateren:** #train = 107,520, #validation = 28,224,
- **CIFAR_{16×16}:** #train = 200,000, #validation = 40,000.

We use the MNIST dataset primarily for the downstream classification task. After the training is done, we use the following train/validation split to evaluate the models:

- **K-nearest neighbor classification** (tables 3 and 5): For this task, we only make use of the validation set for both training and testing of the classifier. We divide up the $N = 10,000$ validation samples into two disjoint sets of $N = 5,000$ samples each. We then draw random samples (without replacement) from the first half and use them for training the KNN classifier. We then test the performance on the other half.
- **Shattering dimensionality** (tables 3 and 5, last column): We use the entire MNIST training set ($N = 60,000$ samples) to train logistic regression classifiers on extracted representations. We then test the results using the entire validation set ($N = 10,000$ samples).

A.2 Architecture details

For sparse coding results, we focused on models with linear decoders. For the fully linear models (Figs. 2 and 5) both the encoder and decoder were linear layers, without bias.

For the convolutional components, we use residual layers without batch norm. For van Hateren and CIFAR_{16×16} datasets, the encoders had 5 layers ($2 \times$ conv each). The decoders had 8 convolutional layers ($1 \times$ conv each). For the MNIST dataset, the encoders had 7 layers ($2 \times$ conv each). The decoders had 10 convolutional layers ($1 \times$ conv each). For all convolutional encoders, the output from ResNet was followed by a learned pooling layer. The pooled output was then fed into a feed-forward layer inspired by Transformers [115], which includes a layer norm as the final operation, the output of which was fed into a linear layer that projects features into posterior distribution parameters. For all convolutional decoders, nearest neighbor upsampling was performed to scale up the spatial dimension of reconstructions.

We experimented with both leaky_relu and swish activation functions [116, 117], and found that swish consistently outperformed leaky_relu in all our experiments across datasets and VAE models.

Please see our code for the full architecture details.

A.3 Training: VAE models

We used a variety of learning rates and batch sizes, depending on the dataset and architecture. For linear models, we used $lr = 0.005$, and for fully conv models we used $lr = 0.002$. All models were trained using the AdaMax optimizer [118] with a cosine learning rate schedule [119]. Please see our code for the full details of training hyperparameters.

KL annealing. For all VAE models, we annealed the KL term during the first half of the training, which is known to be an effective trick in training VAEs [2, 33, 120–122].

Temperature annealing. For discrete VAEs (\mathcal{P} -VAE, \mathcal{C} -VAE), we also annealed the temperature from a large value to a smaller value during the same first half of training. We found that the specific functional form of temperature annealing (e.g., linear, exponential, etc) did not matter as much as the final temperature. For both \mathcal{P} -VAE and \mathcal{C} -VAE, we start from $T_{\text{start}} = 1.0$ and anneal down to $T_{\text{stop}} = 0.05$ for \mathcal{P} -VAE, and $T_{\text{stop}} = 0.1$ for \mathcal{C} -VAE. We found that the \mathcal{C} -VAE performance was not very sensitive to the choice of T_{stop} , corroborating previous reports [88, 97].

The \mathcal{P} -VAE was relatively more sensitive to the value of T_{stop} , and we found marginal improvements when we went lower than $T_{\text{stop}} = 0.1$ to $T_{\text{stop}} = 0.05$. A possible future direction involves defining separate temperatures for the forward and backward passes. For example, setting the forward T_{stop} to zero after the annealing period might further improve performance. We leave this as future work.

A.4 Training: sparse coding models

To fit LCA and ISTA models, we explored a combination of 6 β schedules (same β as in eq. (1)), 3 numbers of iteration (for inference), 3 learning rates, and 5 different seeds (for dictionary initialization). The code for LCA was obtained from the public python library “lca-pytorch”, and the code for ISTA was obtained from public “sparsecoding” repository of the Redwood Center for Theoretical Neuroscience (with added positive constraints).

We explored learning rates of 1×10^{-1} , 1×10^{-2} , and 1×10^{-3} . We trained all models for 100 epochs. We scheduled the β parameters linearly, starting from β_{start} , and stepped it up every five epochs by β_{step} , until it reached β_{end} . We explored the following β schedules (expressed as $\beta_{\text{start}}:\beta_{\text{end}}:\beta_{\text{step}}$):

$$0.05:0.7:0.1, \quad 0.01:0.1:0.01, \quad 0.1:1.0:0.1, \quad 0.05:0.7:0.05, \quad 0.05:0.5:0.05, \quad 0.1:0.1:0$$

We also explored the inference iteration limits of 100, 500, and 900 iterations. We selected the best fits to include in the main results shown in Figs. 2 and 3.

B Supplementary results

In this section, we include additional results that further support those reported in the main paper, including:

- Table 4: Contains the negative ELBO values for all VAE models with a linear decoder. This table reveals a comparable performance between using Monte-Carlo samples to estimate gradients, versus optimizing the exact loss (see eqs. (4) and (18) to (20)), highlighting the effectiveness of our Poisson parameterization algorithm.
- Figure 4: Uses the same data from the Table 4 to visualize the effects.
- Table 5: Contains the full set of downstream classification results. Related to Table 3.
- Figure 5: Shows how the distribution of KL values (or the norm of decoder weights in the case of linear decoders) can be used to determine dead neurons that don’t contribute to the encoding of information.
- Figure 6: Shows MNIST samples generated from the latent space of different VAE models, as well as their reconstruction performance.

C Full derivations

In this section, we provide a self-contained and pedagogical introduction to VAEs, derive the \mathcal{P} -VAE loss function, and highlight how combining Poisson-distributed latents with predictive coding leads to the emergence of a metabolic cost term in the \mathcal{P} -VAE loss. For the case of a linear decoder, the reconstruction loss assumes a closed-form solution. This means we can compute the gradients analytically, which we can then use to evaluate the Poisson reparameterization trick.

C.1 Deriving the evidence lower bound (ELBO) loss

For completeness, let’s first go over the basics. In this section, we will provide a quick refresher on variational inference and derive the VAE loss from scratch. Suppose the data X are generated from the following generative process:

$$p(X) = \int p(X, Z) dZ = \int p(X|Z)p(Z) dZ. \quad (6)$$

Table 4: The reparameterized gradient estimators work as well as exact ones, across datasets and encoder architectures (linear vs. conv). Note that exact gradients are only computable for linear decoders (see eqs. (18) to (20)). The values are negative ELBO (lower is better), shown as mean \pm 99% confidence interval calculated from $n = 5$ different random initializations. EX, exact, MC, Monte-Carlo, ST, straight-through [105].

Model	van Hateren		CIFAR ₁₆ × 16		MNIST		
	linear	conv	linear	conv	linear	conv	
\mathcal{P} -VAE	EX	168.0 \pm .8	162.4 \pm .2	167.1 \pm .2	162.1 \pm .1	41.5 \pm .1	39.7 \pm .2
	MC	167.2 \pm .1	163.4 \pm .1	167.3 \pm .1	162.9 \pm .2	41.7 \pm .2	40.1 \pm .2
	ST	179.3 \pm .1	179.4 \pm .1	182.3 \pm .1	182.3 \pm .2	44.8 \pm .1	44.2 \pm .1
\mathcal{G} -VAE	EX	160.3 \pm .1	154.4 \pm .1	165.9 \pm .1	149.2 \pm .0	40.6 \pm .1	40.0 \pm .1
	MC	160.3 \pm .1	154.4 \pm .1	165.9 \pm .1	149.2 \pm .1	40.7 \pm .1	40.1 \pm .0
\mathcal{C} -VAE	EX	174.9 \pm .1	186.3 \pm .8	177.1 \pm .1	180.6 \pm .5	56.1 \pm .7	59.1 \pm .0
	MC	170.5 \pm .1	171.9 \pm .2	174.7 \pm .1	176.5 \pm .1	39.7 \pm .2	59.1 \pm .0
	ST	174.2 \pm .2	181.1 \pm .3	180.2 \pm .0	185.6 \pm .2	49.3 \pm .1	63.8 \pm 3.4
\mathcal{L} -VAE	EX	167.3 \pm .0	159.0 \pm .2	170.1 \pm .1	154.3 \pm .1	42.1 \pm .1	41.0 \pm .0
	MC	167.3 \pm .0	159.2 \pm .2	170.1 \pm .1	154.5 \pm .1	42.1 \pm .0	41.0 \pm .0

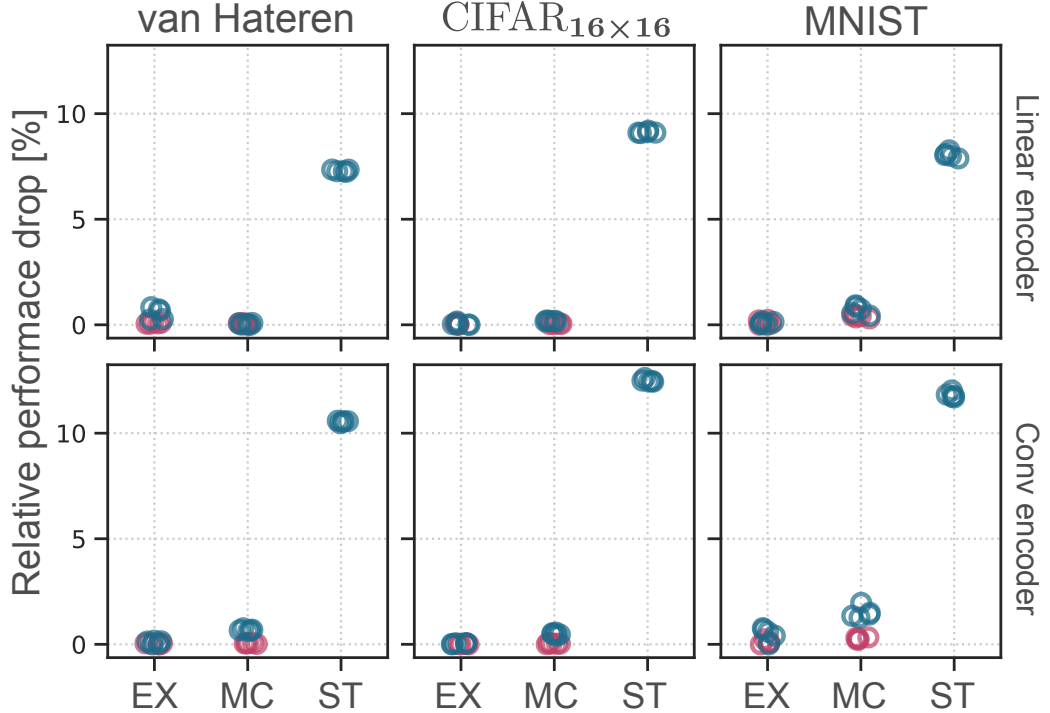


Figure 4: Performance drop relative to the best fit. Blue circles are \mathcal{P} -VAE, and red ones are \mathcal{G} -VAE. There are $n = 5$ circles in each condition, corresponding to 5 random initializations. Using Monte-Carlo samples [123] and our Poisson reparameterization trick (algorithm 1) to estimate gradients performs comparably to the situation where exact gradients are available (see eqs. (18) to (20)). EX, exact, MC, Monte-Carlo, ST, straight-through [105].

The goal of Bayesian inference is to identify which latents Z are likely given data X . In other words, we want to approximate $P(Z|X)$, the true but intractable posterior distribution.

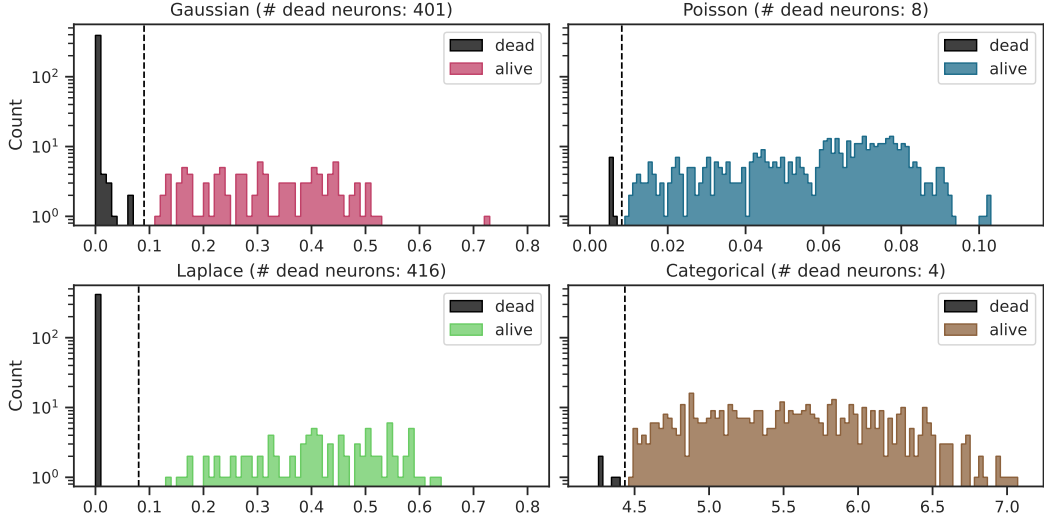


Figure 5: Identifying dead neurons using a histogram-based method. We bin the KL values and determine the gap between small values and larger ones. We identify neurons with KL values lower than the identified threshold (black dashed lines) and pronounce them dead. The figure shows the distribution of KL values over all neurons ($K = 512$) for \mathcal{P} -VAE, \mathcal{G} -VAE, and \mathcal{L} -VAE. The KL term is a single number for the \mathcal{C} -VAE because its latent space consists of a single one-hot categorical distribution with $K = 512$ categories. Therefore, for the \mathcal{C} -VAE, we use the distribution of decoder weight norms instead. These are the same models shown in Fig. 2, where both encoder and decoder are linear. Table 2 uses this method to quantify the proportion of active neurons for VAEs across different datasets and choice of encoder architectures.

Table 5: Geometry of representations. Full set of results. Related to Table 3.

Latent dim.	Model	KNN classification (N , # labeled samples)			Shattering dim.
		$N = 200$	$N = 1,000$	$N = 5,000$	
$K = 10$	\mathcal{P} -VAE	0.815 \pm .002	0.919 \pm .001	0.946 \pm .017	0.797 \pm .009
	\mathcal{C} -VAE	0.705 \pm .002	0.800 \pm .002	0.853 \pm .040	0.795 \pm .006
	\mathcal{L} -VAE	0.757 \pm .003	0.869 \pm .002	0.924 \pm .028	0.751 \pm .008
	\mathcal{G} -VAE	0.673 \pm .003	0.813 \pm .002	0.891 \pm .033	0.758 \pm .007
	\mathcal{G} -VAE _{+relu}	0.694 \pm .003	0.817 \pm .003	0.877 \pm .045	0.762 \pm .007
	\mathcal{G} -VAE _{+exp}	0.642 \pm .003	0.784 \pm .002	0.863 \pm .032	0.737 \pm .008
$K = 50$	\mathcal{P} -VAE	0.825 \pm .002	0.927 \pm .001	0.957 \pm .005	0.935 \pm .003
	\mathcal{C} -VAE	0.770 \pm .002	0.880 \pm .001	0.920 \pm .009	0.899 \pm .004
	\mathcal{L} -VAE	0.710 \pm .003	0.836 \pm .003	0.902 \pm .038	0.770 \pm .007
	\mathcal{G} -VAE	0.604 \pm .003	0.746 \pm .002	0.837 \pm .022	0.743 \pm .007
	\mathcal{G} -VAE _{+relu}	0.710 \pm .002	0.844 \pm .002	0.904 \pm .026	0.786 \pm .006
	\mathcal{G} -VAE _{+exp}	0.694 \pm .003	0.836 \pm .002	0.906 \pm .027	0.762 \pm .007
$K = 100$	\mathcal{P} -VAE	0.807 \pm .002	0.925 \pm .001	0.958 \pm .013	0.949 \pm .002
	\mathcal{C} -VAE	0.753 \pm .002	0.876 \pm .001	0.925 \pm .005	0.884 \pm .004
	\mathcal{L} -VAE	0.701 \pm .004	0.830 \pm .003	0.896 \pm .046	0.767 \pm .007
	\mathcal{G} -VAE	0.636 \pm .003	0.789 \pm .002	0.875 \pm .024	0.763 \pm .007
	\mathcal{G} -VAE _{+relu}	0.757 \pm .002	0.881 \pm .001	0.933 \pm .019	0.818 \pm .006
	\mathcal{G} -VAE _{+exp}	0.695 \pm .003	0.846 \pm .002	0.918 \pm .024	0.793 \pm .006

Variational inference and VAE loss function. To achieve approximate Bayesian inference, a common approach is to define a family of variational densities \mathcal{Q} and find a member $q(Z|X) \in \mathcal{Q}$

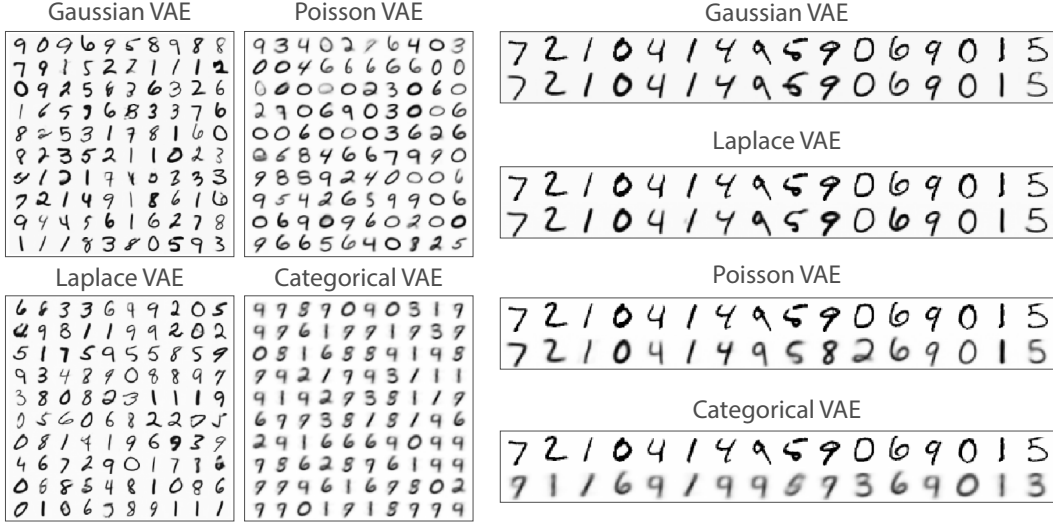


Figure 6: Generated samples (left) and reconstruction performance (right). These results shown here are from fully convolutional (both encoder and decoder) models with a latent dimensionality of $K = 10$.

such that it sufficiently approximates the true posterior. We call $q(Z|X)$ the *approximate posterior*. The general aim of variational inference (VI) can be summarized as follows:

$$\text{VI : } \text{find a } q(Z|X) \in \mathcal{Q} \text{ such that } q(Z|X) \text{ is a good approximation of } p(Z|X). \quad (7)$$

The goodness of our approximate posterior, or its closeness to the true posterior, is measured using the Kullback-Leibler (KL) divergence:

$$q^* = \underset{q \in \mathcal{Q}}{\operatorname{argmin}} \mathcal{D}_{\text{KL}}\left(q(Z|X) \parallel p(Z|X)\right). \quad (8)$$

We cannot directly optimize eq. (8), because $p(Z|X)$ is intractable. Instead, we rearrange some terms and arrive at the following loss function:

$$\mathcal{L}_{\text{NELBO}}(q) = -\mathbb{E}_{z \sim q(Z|X)} \left[\log p(X|Z) \right] + \mathcal{D}_{\text{KL}}\left(q(Z|X) \parallel p(Z)\right). \quad (9)$$

NELBO stands for negative ELBO. Finding a $q \in \mathcal{Q}$ that minimizes $\mathcal{L}_{\text{NELBO}}(q)$ in eq. (9) is equivalent to finding the optimal q^* in eq. (8).

The first term in eq. (9), called the reconstruction term, captures the likelihood of the observed data under the approximate posterior. For all our VAE models, we approximate the reconstruction term as the mean squared error between input data and their reconstructed version, as is typically done in the literature. The second term, known as the KL term, is more interesting. This term can assume very different forms depending on the distribution used.

C.2 The KL term

In this section, we will derive closed-form expressions for the KL term for different choices of the distributions q and p . Specifically, we will focus on Gaussian and Poisson parameterizations.

Predictive coding assumption. We will draw inspiration from predictive coding and assume that the bottom-up inference pathway only encodes the residual information relative to the top-down, or predicted information. We will apply this idea to both Gaussian and Poisson cases, and find that only in the Poisson case, the outcome becomes interpretable and resembles sparse coding.

Gaussian. Suppose $q(z|x) = \mathcal{N}(z; \mu_q(x), \sigma_q(x))$, and $p(z) = \mathcal{N}(z; \mu_p, \sigma_p)$, where the mean and variance are produced either by the encoder network (red) or the decoder network (blue).

Now, let us implement the predictive coding assumption, where the encoder only keeps track of residual information that is not already contained in the prior information. Mathematically, this idea can be formalized as follows:

$$\begin{aligned} \mu_p &\rightarrow \mu, & \mu_q &\rightarrow \mu + \delta\mu \\ \sigma_p &\rightarrow \sigma, & \sigma_q &\rightarrow \sigma \cdot \delta\sigma \end{aligned} \quad (10)$$

With these modifications, the Gaussians KL term becomes:

$$\mathcal{D}_{\text{KL}}(q \parallel p) = \frac{1}{2} \left(\frac{\delta\mu^2}{\sigma^2} + \delta\sigma^2 - \log \delta\sigma^2 - 1 \right). \quad (11)$$

In standard Gaussian VAEs, the prior has no learnable parameter. Instead, we have $\mu \rightarrow \mathbf{0}$ and $\sigma \rightarrow 1$. Therefore, the final form of the KL term for a standard Gaussian VAE is:

$$\mathcal{D}_{\text{KL}}(q \parallel \mathcal{N}(\mathbf{0}, \mathbf{1})) = \frac{1}{2} \left(\delta\mu^2 + \delta\sigma^2 - \log \delta\sigma^2 - 1 \right). \quad (12)$$

We observe that the KL term vanishes when $\delta\mu \rightarrow \mathbf{0}$ and $\delta\sigma \rightarrow 1$. This happens whenever no new information is propagated through the encoder, a phenomenon known as posterior collapse.

Other than this trivial observation, eq. (12) does not really lend itself to interpretation. In contrast, will show below that a Poisson parameterization of VAEs leads to a much more interpretable outcome for the KL term.

Poisson. Now suppose $q(z|x) = \text{Pois}(z; r\delta r(x))$, and $p(z) = \text{Pois}(z; r)$, where z is literally the spike count of a single latent dimension—or shall we say, neuron?

In the Poisson case, the KL term becomes much more interpretable:

$$\mathcal{D}_{\text{KL}}(q \parallel p) = r(1 - \delta r + \delta r \log \delta r) = rf(\delta r), \quad (13)$$

where we have $f(y) := 1 - y + y \log y$.

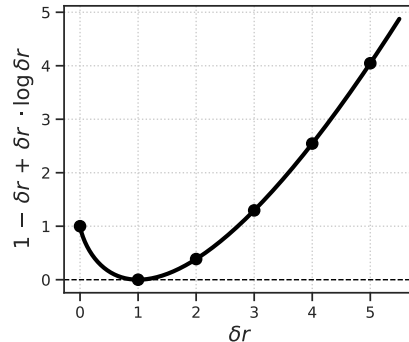
There are two ways to minimize the KL term:

- $r \rightarrow 0$: dead prior neurons.
- $\delta r \rightarrow 1$: posterior collapse.

Figure 7 shows how the residual term (in parenthesis) from eq. (13) depends on the residual firing rate, δr . Together with the reconstruction loss, the NELBO reads:

$$\mathcal{L}_{\text{PVAE}}(r, \delta r) = \mathcal{L}_{\text{recon.}}(r, \delta r) + r(1 - \delta r + \delta r \log \delta r). \quad (14)$$

Figure 7: The residual term f in eq. (13).



C.3 Connection to sparse coding

Equation (14) mirrors sparse coding due to the presence of the firing rate in the objective function. Furthermore, it follows the principle of predictive coding by design. Thus, our Poisson formulation of VAEs effectively unifies these two major themes in theoretical neuroscience. Let's explore this curious connection to sparse coding more closely below.

C.4 Statistically independent neurons

Suppose our \mathcal{P} -VAE has K statistically independent and non-interacting neurons, and $\mathbf{z} \in \mathbb{Z}_{\geq 0}^K$ is the spike count variable, and $\mathbb{Z}_{\geq 0} = \{0, 1, 2, \dots\}$ is the set of non-negative integers. Let us use bold font \mathbf{r} and $\delta\mathbf{r}$ to refer to the firing rate vectors of the [representation](#) and [error](#) units, respectively. Recall that we allowed these variables to interact in a multiplicative way to construct the posterior rates, $\lambda_i(\mathbf{x}) = \mathbf{r}_i \delta\mathbf{r}_i(\mathbf{x})$. More explicitly, we have:

$$\begin{aligned} q(\mathbf{z}|\mathbf{x}) &= \text{Pois}(\mathbf{z}; \mathbf{r} \delta\mathbf{r}) = \prod_{i=1}^K \text{Pois}(z_i; \mathbf{r}_i \delta\mathbf{r}_i) = \prod_{i=1}^K \frac{\lambda_i^{z_i} e^{-\lambda_i}}{z_i!}, \\ p(\mathbf{z}) &= \text{Pois}(\mathbf{z}; \mathbf{r}) = \prod_{i=1}^K \text{Pois}(z_i; \mathbf{r}_i) = \prod_{i=1}^K \frac{\mathbf{r}_i^{z_i} e^{-\mathbf{r}_i}}{z_i!}. \end{aligned} \quad (15)$$

Note that, unlike a standard Gaussian VAE, the prior in \mathcal{P} -VAE is parameterized using \mathbf{r} , which is learned from data along with the other parameters. Similar to standard Gaussian VAEs, $\delta\mathbf{r}(\mathbf{x})$ is parameterized as a neural network.

C.5 Linear decoder

Following the sparse coding literature, we will now assume our decoder generates the input image $\mathbf{x} \in \mathbb{R}^M$ as a linear sum of K basis elements, $\Phi \in \mathbb{R}^{M \times K}$. We approximate the reconstruction loss as the mean squared error between the input \mathbf{x} , and its reconstruction $\Phi\mathbf{z}$. Given these assumptions, the VAE reconstruction loss becomes:

$$\mathcal{L}_{\text{recon.}}(\mathbf{x}; \mathbf{q}) = \mathbb{E}_{\mathbf{z} \sim q(Z|X=\mathbf{x})} \left[\|\mathbf{x} - \Phi\mathbf{z}\|_2^2 \right]. \quad (16)$$

For a linear decoder, the reconstruction term $\|\mathbf{x} - \Phi\mathbf{z}\|_2^2$ contains only the first and second moments of \mathbf{z} . Consequently, the expectation in eq. (16) can be analytically resolved. This yields the loss function, and consequently, its gradients in closed form. Specifically, for the Poisson case, we only need to know the following expectation values:

$$\begin{aligned} \mathbb{E}_{\mathbf{z} \sim \text{Pois}(\mathbf{z}; \boldsymbol{\lambda})} [z_i] &= \lambda_i, \\ \mathbb{E}_{\mathbf{z} \sim \text{Pois}(\mathbf{z}; \boldsymbol{\lambda})} [z_i z_j] &= \lambda_i \lambda_j + \delta_{ij} \lambda_i. \end{aligned} \quad (17)$$

More generally, whenever the VAE decoder is linear, the following result holds:

$$\boxed{\mathcal{L}_{\text{recon.}}(\mathbf{x}; \mathbf{q}, \Phi) = \|\mathbf{x} - \Phi \mathbb{E}_{\mathbf{q}}[Z]\|_2^2 + \text{Var}_{\mathbf{q}}[Z]^T \text{diag}(\Phi^T \Phi).} \quad (18)$$

Note that a linear decoder is the only assumption we needed to obtain this closed-form solution. There are no restrictions on the form of the encoder: it can be linear, or as complicated as we want. We only have to compute the mean and variance of the posterior. Here are the reconstruction losses for both Poisson and Gaussian VAEs with linear decoders, put side-by-side for comparison:

$$\boxed{\begin{aligned} \text{Poisson:} \quad \mathcal{L}_{\text{recon.}}(\mathbf{x}; \boldsymbol{\lambda}, \Phi) &= \|\mathbf{x} - \Phi \boldsymbol{\lambda}\|_2^2 + \boldsymbol{\lambda}^T \text{diag}(\Phi^T \Phi), \\ \text{Gaussian:} \quad \mathcal{L}_{\text{recon.}}(\mathbf{x}; \boldsymbol{\mu}, \boldsymbol{\sigma}, \Phi) &= \|\mathbf{x} - \Phi \boldsymbol{\mu}\|_2^2 + (\boldsymbol{\sigma}^2)^T \text{diag}(\Phi^T \Phi). \end{aligned}} \quad (19)$$

Given these assumptions, the NELBO (eq. (14)) for \mathcal{P} -VAE with a linear decoder becomes:

$$\boxed{\mathcal{L}_{\text{SC-PVAE}}(\mathbf{x}; \delta\mathbf{r}, \mathbf{r}, \Phi) = \|\mathbf{x} - \Phi \boldsymbol{\lambda}\|_2^2 + \boldsymbol{\lambda}^T \text{diag}(\Phi^T \Phi) + \beta \sum_{i=1}^K \mathbf{r}_i f(\delta\mathbf{r}_i).} \quad (20)$$

Recall that we have $f(y) = 1 - y + y \log y$ (see Fig. 7). We introduced the β term here to control the trade-off between the reconstruction and the KL term. Additionally, we dropped the explicit dependence of $\delta r(x)$ on the input image x to increase readability.

C.6 Linear encoder

We can further simplify the \mathcal{P} -VAE architecture by making the encoder also linear. Let's use $\mathbf{W} \in \mathbb{R}^{K \times M}$ to denote encoder weights, and assume an exponential link function mapping the input into the residual firing rates. In other words, we have $\delta r = \exp(\mathbf{W}x)$. To obtain the final form of the loss function, we start from eq. (20), plug in $\log(\delta r) = \mathbf{W}x$, and rearrange some terms to find:

$$\mathcal{L}_{\text{VAE}} = \boldsymbol{\lambda}^T \Phi^T \Phi \boldsymbol{\lambda} + \boldsymbol{\lambda}^T \text{diag}(\Phi^T \Phi - \beta \mathbf{I}) + \boldsymbol{\lambda}^T (\beta \mathbf{W} - 2\Phi^T) \mathbf{x} + \beta \sum_{i=1}^K \mathbf{r}_i + \mathbf{x}^T \mathbf{x}. \quad (21)$$